Applied Surface Science 612 (2023) 155734

Contents lists available at ScienceDirect

Applied Surface Science

journal homepage: www.elsevier.com/locate/apsusc

Full length article

Artificial intelligence based analysis of nanoindentation load–displacement data using a genetic algorithm

Abraham Burleigh [a], Miu Lun Lau [b], Megan Burrill [c], Daniel T. Olive [d], Jonathan G. Gigax [d], Nan Li [d], Tarik A. Saleh [d], Frederique Pellemoine [e], Sujit Bidhar [e], Min Long [b], Kavin Ammigan [e], Jeff Terry [a,c,f,*]

[a] Department of Physics, Illinois Institute of Technology, Chicago IL 60616, United States of America
[b] Department of Computer Science, Boise State University, Boise ID 83725, United States of America
[c] Department of Mechanical, Materials, and Aerospace Engineering, Illinois Institute of Technology, Chicago IL 60616, United States of America
[d] Los Alamos National Laboratory, Los Alamos NM 87545, United States of America
[e] Fermi National Accelerator Laboratory, Batavia IL 60510, United States of America
[f] Department of Social Sciences, Illinois Institute of Technology, Chicago IL 60616, United States of America

ARTICLE INFO

Keywords:
Nanoindentation
Artificial intelligence
Genetic algortithm

ABSTRACT

We developed an automated tool, `Nanoindentation Neo` package for the analysis of nanoindentation load–displacement curves using a Genetic Algorithm (GA) applied to the Oliver-Pharr method (Oliver et al.,1992). For some materials, such as polycrystalline isotropic graphites, Least Squares Fitting (LSF) of the unload curve can produce unrealistic fit parameters. These graphites exhibit sharply peaked unloading curves not easily fit using the LSF, which tends to overestimate the indenter tip geometry parameter. To tackle this problem, we extended our general materials characterization tool `Neo` for EXAFS analysis (Terry et al., 2021) to fit nanoindentation data. `Nanoindentation Neo` automatically processes and analyzes nanoindentation data with minimal user input while producing meaningful fit parameters. GA, a robust metaheuristic method, begins with a population of temporary solutions using model parameters called chromosomes; from these we evaluate a fitness value for each solution, and select the best solutions to mix with random solutions producing the next generation. A mutation operator then modifies existing solutions by random perturbations, and the optimal solution is selected. We tested the GA method using Silica and Al reference standards. We fit samples of graphite and a high entropy alloy (HEA) consisting of BCC and FCC phases.

1. Introduction

Nanoindentation is a technique well suited to probing mechanical properties because it can extract hardness and elastic modulus values from very shallow regions of a sample on the order of microns. During the nanoindentation process materials undergo two types of material deformation: plastic and elastic [1]. For a fully elastic deformation, as seen in the load displacement curve of Fig. 1(a) for fused silica the material is able to fully recover its original shape (for sufficiently small indents) resulting in an unloading curve that closely traces the loading. At the other extreme, a completely plastic deformation results in an unloading curve that is nearly vertical as the material fails to recover leaving a large residual indent to nearly the full depth as shown for single crystal aluminum in Fig. 1(b).

Fine grained, isotropic graphite grades are utilized in many current and future fixed target, high-energy proton beam experiments for neutrino production [2–5]. Low-Z materials produce favorable secondary particle spectra optimal for neutrino production [5,6], and graphite offers strong resistance to thermal shock [4,7] which is a major concern for pulsed beam targets that experience a drastic increase in mechanical load due to the sharp thermal gradient during pulses. During nanoindentation some samples, such as fine grained, polycrystalline graphite, show recovery properties exhibiting regions of both elastic and plastic deformation as shown in Fig. 2 where the unloading curve is sharply peaked near the maximum load and then recovers midway through the unloading process resulting in a drastic change in the slope of the curve. This makes fitting the unloading portion of the load displacement curve difficult using a Least Squares Fitting (LSF) process as discussed in Section 2.1. Our Genetic Algorithm (GA)-based fitting process is able to fit this data accurately and efficiently while producing fitting parameters that are physically meaningful and consistent with theory.

* Correspondence to: 3101 S. Dearborn St., Chicago IL 60616, United States of America.
E-mail address: terryj@iit.edu (J. Terry).

https://doi.org/10.1016/j.apsusc.2022.155734
Received 10 August 2022; Received in revised form 2 November 2022; Accepted 14 November 2022
Available online 17 November 2022

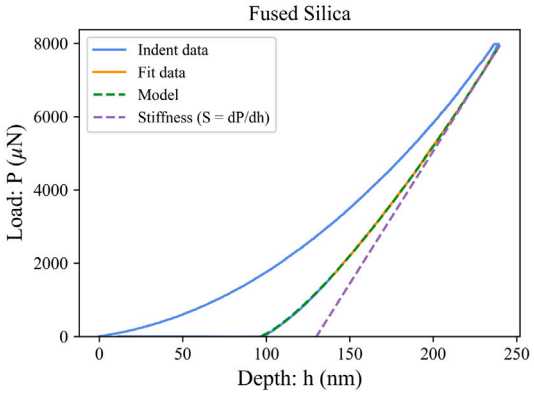

(a) Fused silica shows a highly elastic response and strong material recovery as the loading and unloading curves nearly overlap.

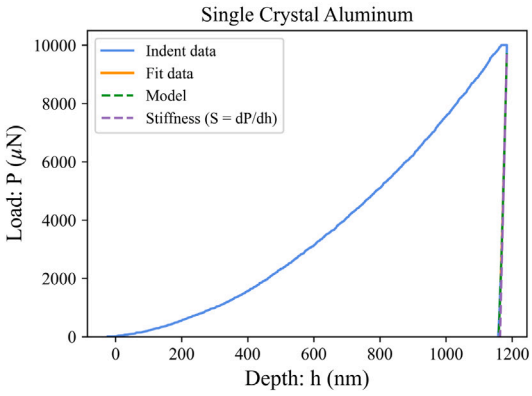

(b) Single crystal aluminum displays plastic deformation and almost no material recovery given the nearly vertical response of the unloading curve.

Fig. 1. Nanoindentation load/unload curves from indentations on fused silica and single crystal aluminum.

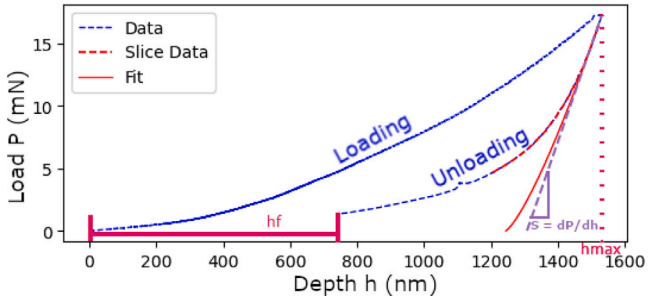

Fig. 2. Representative load/unload curve from nanoindentation of ion irradiated graphite (Fit data annotated as in [1]).

2. Methodology

2.1. Nanoindentation

Analysis of nanoindentation data can be done by examining the load/unload curve during indentation using the Oliver-Pharr method, or by continuous stiffness measurements (CSM) [1]. The results of our GA fitting package will be compared to those of CSM for identical indentations in the following section. The nanoindentation unloading data is found to be well described by the power law expression [1]:

$$P = A(h - h_f)^m \tag{1}$$

where A, h_f, and m are all free parameters (discussed in detail below) that will be determined by the GA. The independent parameters used in the fitting process are h, the indentation depth, and P, the indenter load. For both nanoindentation analysis methods, we are predominantly concerned with determining the elastic modulus E and hardness H. For determination of these parameters from the load/unload curve, we use the following equations [1]:

$$\frac{1}{E_r} = \frac{1-\nu^2}{E} + \frac{1-\nu_i^2}{E_i}, \tag{2}$$

$$H = \frac{P_{max}}{A(h_c)}, \tag{3}$$

where E_r is the experimentally determined reduced modulus which accounts for displacement of both the sample and indenter tip, E_i and ν_i are the modulus and Poisson's ratio of the indenter tip (commonly diamond), respectively. The Poisson's ratio of the sample, ν is taken from the literature or measured before the nanoindentation measurement [1]. P_{max} is the maximum load during indentation and $A(h_c)$ is the indenter contact area as a function of peak indentation depth given by [1,8,9]:

$$A(h_c) = 24.5h_c^2 + C_1h_c^1 + C_2h_c^{1/2} + C_3h_c^{1/4} + \cdots + C_8h_c^{1/128}. \tag{4}$$

The constants C_1 - C_8 are determined for a particular indenter tip by performing indentations on a well characterized material such as fused silica, and h_c is the vertical contact distance. The vertical contact distance h_c used to determine the contact area takes into account the fact that there is a region of deformation at the surface that does not contact the indenter tip which is given by h_s:

$$h_s = \epsilon\frac{P_{max}}{S}. \tag{5}$$

The contact depth h_c is therefore related to the maximum indentation depth by:

$$h_{max} = h_c + h_s. \tag{6}$$

The geometric constant ϵ is 0.75 for a Berkovich tip [1,10], and S is the material stiffness during initial unloading given by [11–15]:

$$S = \frac{dP}{dh} = 2E_r\sqrt{\frac{A(h_c)}{\pi}} \tag{7}$$

which can be determined by fitting the upper portion of the unloading curve using Eq. (1) and evaluating the first derivative at the maximum load and depth giving a straight line approximation through the maximum load position as shown in Fig. 2. The stiffness as determined from the fitting parameters is then:

$$S = Am\left(h_{max} - h_f\right)^{m-1} \tag{8}$$

In Eq. (1), the fitting parameter, A, is a material constant that gives a scaling factor that cannot be directly correlated to a feature of the load/unload curve [1]. The parameter, h_f, is a measure of the residual indentation depth on unloading after the tip has been withdrawn [1, 16], which can also be directly observed from the load/unload curve as it crosses the depth axis as shown in Fig. 2. The parameter m is dependent on the indented material and indenter tip shape; it corresponds to the geometry of the contact area between the two [1,10]. If we assume a linear unloading sequence for indentations using a flat cylinder (or flat punch), we will have $m = 1$, and $m = 2$ for a cone shaped tip and between these extremes a paraboloid of revolution has $m = 1.5$ [1,10,17]. It also has been shown by elastic contact theory [12,16], finite element analysis [18] and experiment [12] that determination of the stiffness using Eq. (7) is also valid for pyramidal tip shapes such as the Vickers

and Berkovich tip used in our measurements. For indentations analyzed according to the above theory that do not display linear unloading the process is best described by using an exponent m that is roughly between 1.2–1.6 for most tip geometries and materials [1].

For the related CSM experiments, the indenter tip oscillates during loading with an amplitude on the order of nanometers. The system is modeled as two springs (stiffness: $[C_f + \frac{1}{S}]^{-1}$ and K_s) in parallel with a damping term D attached to indenter tip of mass m [1,19,20], so that

$$\left|\frac{P_{os}}{h(\omega)}\right| = \sqrt{\left([S^{-1} + C_f]^{-1} + K_s - m\omega^2\right)^2 + \omega^2 D^2}. \quad (9)$$

Here C_f [m/N] is the load frame compliance, K_s the support spring stiffness [N/m], and D [s/m] the damping coefficient of the capacitive plate used to measure displacement, all of which are determined during instrument calibration. P_{os} and $h(\omega)$ are the magnitude of load and depth oscillation respectively, ω the oscillation frequency, and m the indenter tip mass. K_s and D can be determined from oscillations of the system when not in contact with the surface (S=0), and then determination of the material stiffness depends only on the measured oscillation depth $h(\omega)$ for a given load P_{os} which can be determined at any depth from the surface up to h_{max}.

2.2. Genetic algorithms

Genetic Algorithms [21] are a class of efficient metaheuristic methods for optimizing highly non-convex objective functions, inspired by processes of biological evolution. GA operates on a population of N individuals ($\mathcal{P}_i$), each of which represents a set of solution points (e.g., physical parameters) in the solution domain. Each individual is evaluated by the use of a fitness value which is determined using an objective function. During each iteration (i.e., a *generation*) of the algorithm, a new population is generated such that the average individuals will have superior fitness values compared to previous generation. The use of a diverse population combined with genetic inspired operators (crossover and mutation) enables GA to properly explore any high-dimensional domains, while reducing the chance of trapping in local minima.

Our Genetic Algorithm used for the nanoindentation fitting below is being released as open source software. The algorithm was originally developed for the fitting of extended X-ray absorption fine structure (EXAFS) data [22,23]. The open source EXAFS Neo package can be downloaded on Github [24]. Our nanoindentation fitting program, `Nanoindentation Neo`, is also available on Github [25]. `Nanoindentation Neo` requires the user to select the limits of parameter space that are appropriate for the materials that have been probed by the nanoindentation machines. Our objective function relies on optimizing the equation described by Eq. (1). Our algorithm creates an initial *population* of the three parameters (A, h_f, and m from Eq. (1)) associated with each of the individuals. The objective fitness is determined by comparing the model data to the experimental data using Eq. (10) and used to determine the fitness of the populations in each generation by computing the difference between the sum of the squares of the experimental data, $Expt_i$, and the calculated result from the GA Model, $Model_i$. To prevent over-fitting of the experimental data, the reduced chi squared, χ_r^2, is used to determine the goodness of fit, where N_{ind} is the number of independent data points, N_{params} is the number of fitting parameters, and N is the total number of data points. ϵ_i is assumed to be 1 since it is difficult to determine the error of each point. The resulting set of populations are sorted based on their fitness score using:

$$\chi_r^2 = \frac{N_{ind}}{(N_{ind} - N_{params})\,N} \sum_{i=1}^{N} \frac{(Expt_i - Model_i)^2}{\epsilon_i^2}. \quad (10)$$

Our GA has been described in detail [22,23] and will only be summarized here. The goal of the GA is to find an individual, P_{best}, that best minimizes the difference between the theoretical measurement

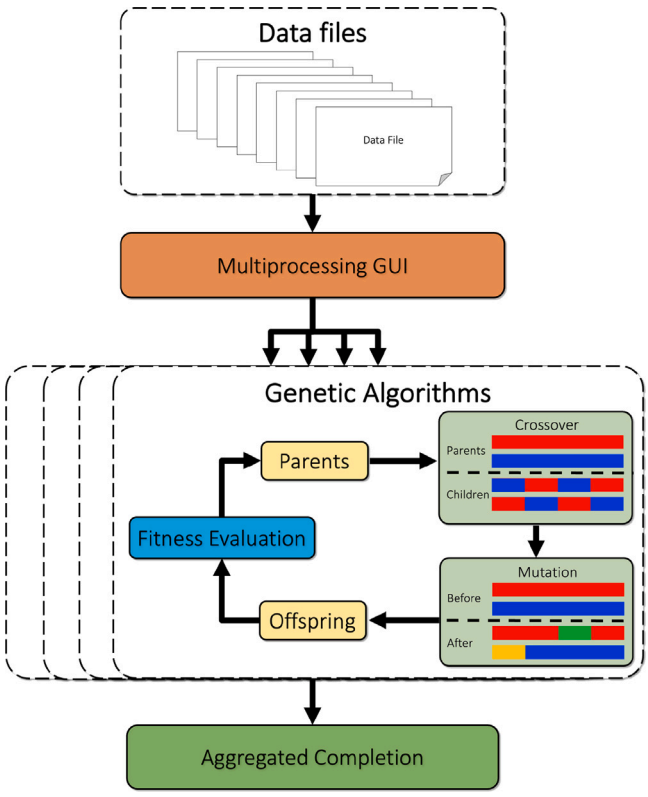

Fig. 3. A schematic of the iterative structure of the GA of our `Nanoindentation Neo`. A number of nanoindentation file is first input using a user-friendly graphical user interface (GUI) of the package, in which each data file gets separated and enters into its own analysis subroutine consisting of a GA. Inside the GA, a population consisting of N individuals is entered into a fitness evaluation loop where *Cross-Over* and *Mutation* operators are used to improve the diversity and ultimately the fitness, $f(\mathcal{P}_i)$, until one of the termination conditions is reached. Afterward, each sample is analyzed which returns the physical values such as hardness and modulus. This result can then be further aggregated and provide an overall result for the sample.

calculated from its set of parameters and the observed data. The fitness of each individual $f(\mathcal{P}_i)$ is computed as reciprocal of the sum-of-squared-error (SSE) between its predicted against the observed data. In the GA, individuals with higher fitness will have greater probability of being retained and selected as potential parents of individuals in the next population. These subsequent individuals are generated using both *Cross-over* and *Mutation* operators. A schematic of the GA is shown in Fig. 3. The software we have written parses inputs using a input file, which contains all analysis and processing parameters. The software process inputs from the input file and then perform the calculations. This setup permits the submissions of multiple input scripts simultaneously to allow for high throughout. The accelerated workflow also suits very well with the parallel job submissions capabilities in High Performance Computing (HPC). HPC systems at INL (sawtooth) were employed for the analysis sections. Since each individual analysis does not require huge computational resources, minimal CPU hours were requested (typically 4-core, and a wall time of 30 min). Instead, a large amount of jobs are typically submitted to take advantages of the parallelism.

The *Cross-Over* operator combines two individuals, $\mathcal{P}_a$ and $\mathcal{P}_b$, by choosing random subsets of parameters from each, subject to constraints, and returning their union. The *Mutation* operator, with some probability (*mutation rate*), randomly changes one of the three parameters (A, h_f, and m) in the individual. The mutation rate is randomly adjusted depending upon the success rate of the generations using the Rechenberg mutation rate adaptation [26] algorithm. The Rechenberg algorithm dynamically alters the mutation rate depending on the

Table 1
Global random analysis ranges and step size.

Parameters	Minimum	Maximum	Step size
Populations	100	3000	100
Generations	20	100	10
Mutation Chance	20%	100%	10%

number of successful mutations (those whose offspring have increased fitness). This improvement led to a factor of 10 decrease in the number of generations required to achieve convergence. Termination of the GA can be accomplished by reaching either of two endpoints. The first is when the maximum number of generations set by the user is reached. This "cut-off" option is designed to provide users a threshold time step to end the calculation to save computing resources. The second occurs when the fitness of individuals in subsequent generations has converged to a self consistent level for a user defined percentage, ($K\%$) of the total generations. In general, successive populations should increase the average fitness value of the population, and hence, over time, generate a population comprising many individuals with high fitness and therefore low SSE. The final output of the algorithm is the best fitted individual from the last population.

The analysis package containing the GA code is called `Nanoindentation Neo` [25]. It is an open source application written in the Python [27] programming language. There is no emerging need to parallelize our GA code (though it could be) since the same data set should be run/analyzed multiple times independently to gauge the errors compared to the experiments. Thus, we strongly recommended that users execute multiple calculations simultaneously for doing such error analysis. The available GUI can be used to populate multiple random parameter sets for simultaneous exploration of the parameter space as well as serial execution of searches of allowed parameter space. The multiple solutions could be used in the error analysis described below.

2.3. Error analysis

Our algorithm does not optimize the population size, the number of children from each set of parents, the number of parents in each generation, starting mutation probability, or the number of generations. We use variations in the starting values of these parameters to generate a number of solutions with different initial conditions to evaluate the error in the optimal path parameters. Global random analysis [28,29] was performed to determine these error ranges. Random perturbations were applied to the parameters *Population Size*, *Number of Generations*, and *Mutation Chance*, and the GA was run for up to 100 different perturbations for each sample. The ranges and step sizes of each parameter are shown below in Table 1. The set of result values generated from the different runs were used to further compute the co-variance matrix which results in the potential errors of each independent variable. All listed errors are the statistical errors of the AI analysis routine. They detail the accuracy and precision of the GA.

3. Results and discussion

3.1. Reference material fitting

The GA-based `Nanoindentation Neo` was used to analyze data from two common reference materials that have been extensively studied: fused silica and single crystal aluminum. Fused silica is commonly used to determine the coefficients of the contact area function given by Eq. (4) due to its highly elastic recovery during unloading. Single crystal aluminum can be used for calibrating the spatial offset between imaging hardware and indenter tip due to its easily observable residual contact area after unloading. The results of GA fits performed on sets of 9 indentations in fused silica and aluminum samples are shown in Table 2. Both sets of indentations were performed using Hysitron TI-950 Triboindenters; the fused silica on an instrument at Northwestern NUANCE (NUANCE), and the aluminum on an instrument at Los Alamos National Laboratory (LANL).

In the case of fused silica the indentations were done to a maximum load of 8000 μN. Indentation #1 and #3 penetrated the material to 330.3 nm and 492.2 nm respectively - a much greater peak depth than the other 7 tests which reached an average maximum depth of 238.5 ± 0.7 nm. The calculated hardness and elastic modulus results for indentations #1 and #3 are correspondingly low compared to the rest of the tests bringing down the average values and increasing the experimental uncertainties for both properties. The GA fitting calculated hardness value (8000 ± 3000 MPa) falls within the range of values found in the literature of 7000–9500 MPa [1,30,31]. The elastic modulus (70 ± 20 GPa) is also within the range 69–72 GPa found in the literature [1,30,32]. If the 2 outlier measurements are excluded from the set the average hardness increases to 9980 ± 60 MPa, and the average elastic modulus increases to 74.8 ± 0.7 GPa; values slightly higher than the literature in both cases. The average value for the parameter m is ≈ 5% higher than the value of 1.25 given by the experiments of Oliver and Pharr for fused silica [1]. Applying a LSF procedure to this data yields comparable results for the hardness (8376.0 ± 3157.0 MPa) and elastic modulus (65.94 ± 16.34 GPa) which increase to 9932.6 ± 63.8 MPa and 73.86 ± 0.43 GPa respectively if the outliers are excluded. When comparing the two types of fitting procedures both material properties fall within 1σ of each other with and without inclusion of the outliers. The average GA fitness score (discussed in Section 2.2) for the indentations in this set is 1.117×10^{15} which is somewhat better than the LSF fitness value of 1.889×10^{15} when the same algorithm is applied to each set of fit parameters.

For the aluminum tests a maximum load of 10000 μN was used corresponding to an average peak indentation depth of 1178.7 ± 5.6 nm across all tests. The GA computed average hardness (279 ± 3 MPa) compares well with values in the literature of 250–330 MPa [1] and is within experimental error when compared to the values given by Filippov of 262.4 ± 13.6 MPa for the hardness averaged over all crystallographic orientations [33]. Likewise the elastic modulus (69 ± 2 GPa) falls within 1σ of the range of values from the literature of 67.1–70.4 GPa [1,34], and most closely matches the modulus along the (110) direction calculated by Filippov to be 72.0 GPa [33]. The results of Oliver and Pharr give $m = 1.38$ for indentations in aluminum [1] which is 2.3% larger than the parameter found by the GA and within the experimental error of this value. Fig. 4 shows graphically how the calculated values of m for fused silica and aluminum compare to those from the literature. LSF fitting done by the Hysitron instrument calculates a hardness of 311.8 ± 3.0 MPa and elastic modulus of 73.14 ± 2.32 GPa. The LSF hardness is significantly higher than the GA value as well as that given by Filippov, but the modulus values are within one standard deviation of each other. The average GA fitness score for this set of data is 1.737×10^{18} which is again an improvement on the LSF fitness score of 4.819×10^{20}.

3.2. GA fitting of graphite

3.2.1. Comparison with LSF

Nanoindentation measurements were performed using a Hysitron TI-950 Triboindenter at NUANCE on POCO ZXF-5Q fine grained, isotropic graphite to a maximum load of 10.0 mN corresponding to an indenter displacement at peak load of 1024–1506 nm depending on the local hardness for a particular indentation. LSF of the load/unload curve using the Oliver-Pharr method returned values of the material hardness in agreement with the values found in the literature of H = 200–400 MPa [35–37] while elastic modulus values are at the low end of the accepted range of E = 9.1–10.5 GPa for fine grained, isotropic polycrystalline graphite grades [35,38–40]. Additionally the calculated fit parameters h_f and m do not fall within the range of acceptable values described by the theory of load displacement analysis

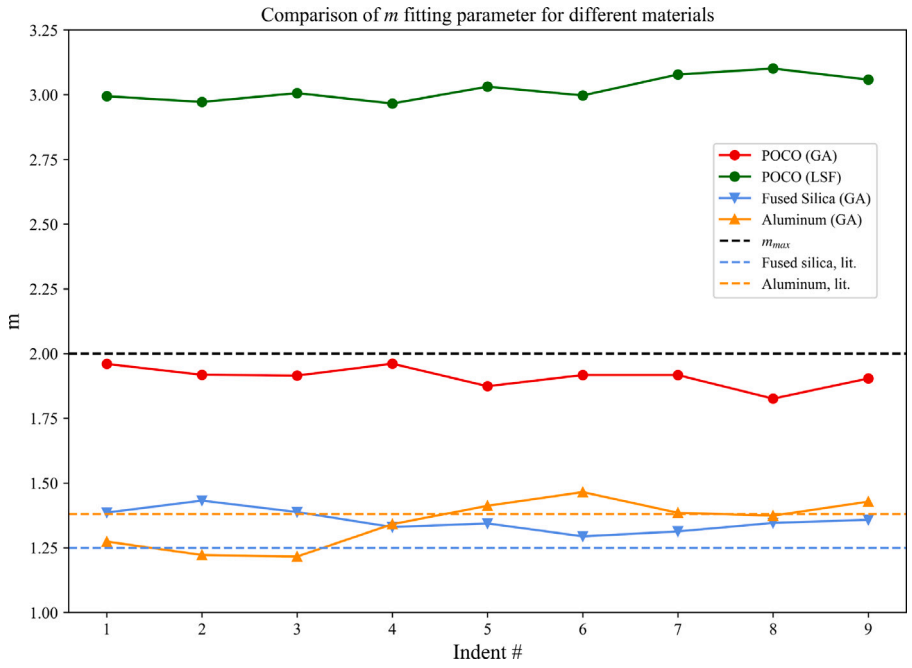

Fig. 4. Values of the power law exponent parameter m as defined by the Oliver-Pharr method described in Section 2.1 for POCO graphite calculated using the GA software (red, point) and LSF (green, point) fitting, and Fused Silica (blue, down triangle) and Aluminum (orange, up triangle) using the GA. The black horizontal dashed line shows the maximum value of m as defined by the theory behind the Oliver-Pharr method while the blue and orange horizontal lines show the values of m for Fused Silica and Aluminum from the literature respectively [1]. For POCO graphite, the GA finds values of m within the range predicted by theory, while the LSF values greatly exceed it. The values found for fused silica and aluminum are similar to those from the literature.

Table 2
Hardness and modulus results for GA fits of fused silica and single crystal Al reference materials.

Indent	Fused silica					Aluminum				
	A (μN/nm^m)	h_f (nm)	m	H (MPa)	E (GPa)	A (μN/nm^m)	h_f (nm)	m	H (MPa)	E (GPa)
1	7.58	181.2	1.386	4252.3	47.58	154.4	1158.1	1.274	274.63	66.40
2	5.89	85.6	1.432	9892.2	75.72	187.4	1149.3	1.222	281.31	65.45
3	7.59	344.2	1.388	1636.0	29.39	196.6	1153.1	1.216	279.72	66.70
4	10.63	94.0	1.33	10034.9	75.10	120.5	1149.3	1.341	280.52	69.18
5	9.78	92.7	1.344	9979.1	74.93	92.3	1148.8	1.412	280.43	71.23
6	12.91	97.2	1.294	10006.3	73.76	73.2	1138.7	1.465	284.49	71.84
7	11.64	95.9	1.313	9941.9	74.12	102.5	1156.9	1.385	276.61	70.11
8	9.61	91.9	1.346	10070.9	74.89	106.2	1156.1	1.374	276.79	69.39
9	9.05	91.8	1.358	9951.3	75.18	84.8	1155.1	1.428	277.28	70.19
Avg.	9	130	1.36	8000	70	120	1152	1.35	279	69
St. Dev.	2	90	0.04	3000	20	40	6	0.09	3	2

discussed in Section 2.1. Table 3 shows the results obtained from the LSF compared to those of the GA for the same set of 9 indentations. Both fitting algorithms used data points from the top 50% of the unload curve. The calculated hardness values are within the degree of experimental error when calculated with both methods. According to Eq. (3) the hardness depends only on peak load and the contact area at maximum depth which is less dependent on the calculated stiffness value compared to the elastic modulus found using Eqs. (7) and (2). On average the hardness value from GA fitting is 1.2% larger compared to the LSF, while the elastic modulus is 5.3% smaller. The standard deviation of the hardness results is nominally the same for both cases (27.6% for the LSF, 27.7% for the GA) as is the standard deviation for the elastic modulus (20.6% for the LSF, 20.2% for the GA). The hardness results are near the center of the published range of results [35–37] and the elastic modulus results near the bottom of the published range of values [35,38–40]. Examination of the curves in Figs. 10 and 11 shows that indentations exhibiting larger hardness and elastic modulus values penetrate to greater depths when compared to indentations with low hardness and elastic modulus results. This variation in the maximum indentation depth for a fixed peak load points to the observed deviation being the result of differing material properties across the sample surface as opposed to inconsistencies in the fitting process.

Table 3
The LSF and the GA results agree within the degree of experimental error for the POCO ZXF-5Q graphite sample.

Indent	Least Sq.		GA	
	H (MPa)	E (GPa)	H (MPa)	E (GPa)
1	371.57	10.29	375.06	9.93
2	333.95	9.34	338.16	8.91
3	302.49	9.42	305.87	8.98
4	208.52	7.68	211.04	7.22
5	263.52	10.10	266.45	9.52
6	206.61	7.70	208.67	7.31
7	425.14	14.03	431.43	13.14
8	192.44	7.81	193.95	7.47
9	317.60	9.64	323.71	8.92
Avg.	290	10	290	9
St. Dev.	80	2	80	2

When examining the physically meaningful parameters generated by both types of fitting shown in Table 4, the LSF greatly overestimate

Table 4
For the set of 9 indentations in POCO ZXF-5Q polycrystalline graphite, the LSF consistently produces unrealistic values for the indenter shape parameter m while GA fit parameters fall in physically realistic ranges given by the theory.

Indent	Least Sq.			GA		
	A (μN/nm^m)	h_f (nm)	m	A (μN/nm^m)	h_f (nm)	m
1	1.004E−04	652.3	2.994	0.1210	799.4	1.960
2	1.035E−04	696.2	2.972	0.1440	848.6	1.918
3	9.596E−05	765.9	3.006	0.1650	916.8	1.915
4	1.188E−04	992.9	2.966	0.1140	1133.5	1.961
5	1.213E−04	885.9	3.031	0.2750	1024.6	1.874
6	9.892E−05	1000.2	2.997	0.1580	1149.8	1.917
7	1.119E−04	644.8	3.078	0.2410	773.0	1.917
8	5.493E−05	1051.2	3.101	0.3240	1225.4	1.826
9	6.557E−05	729.4	3.058	0.1670	882.6	1.904
Avg.	9.680E−05	824.3	3.023	0.19	1000	1.91
St. Dev.	2.264E−05	160.2	0.047	0.07	200	0.04

the value of m which according to the theory should be at most 2.0 and is expected to fall between 1.2 and 1.6. The mean value of m found by the LSF is 3.02 with a standard deviation of 0.05. When a limit for the range of m of 1.0–2.0 is applied it results in every fit finding a solution with $m = 2.0$, this is also the case for applying an upper limit of 1.6. This effectively removes one of the free parameters from the fitting process and results in the user manually choosing a value for m. The GA software can find fitting parameters m for this set of indentations that match the expected range with a mean value of 1.91 and a standard deviation of 0.04; this discrepancy between the two fitting algorithms is shown in Fig. 4. The ability of the GA method to find fitting parameters that are consistent with the theory behind the Oliver-Pharr method increases confidence that the results are accurate. The values for h_f also vary between the two fitting algorithms, and in both cases corresponds to a larger depth than the intersection of the unloading curve with the depth axis. Figs. 10 and 11 in the Appendix show the plots for each fit given by the GA and LSF respectively and show graphically the relation between h_f and the shape of the unloading curve. For all indentations examined the GA fit value of h_f is larger than that of the LSF, as is the parameter A. This is a result of the fact that the exponent m is smaller, so the fit peaks upward more gradually. Therefore, the scaling factor A and the depth axis intercept h_f are greater in order to bring the fitted model into the range of the data points. The GA fitting finds values of h_f that correspond to the inflection point where graphite's material response and the slope of the unloading curve change over to display a more elastic response. For the LSF, h_f corresponds to a depth intermediate between the inflection point and the unload curve's intercept with the depth axis. For indentations #3 and #5 which show minimal elastic response at the end of unloading h_f is closely aligned with the intercept.

3.2.2. Comparison with continuous stiffness measurements (CSM)

Continuous stiffness measurements (CSM) were performed on a pristine IG-430 polycrystalline graphite sample using a KLA iMicro nanoindentation system at Fermi National Accelerator Laboratory (FNAL) to a maximum displacement at peak load of 1500 nm which corresponds to peak loads of 11.8–21.4 mN the value of which is again dependent on the varying hardness of the graphite at a particular indentation location. IG-430 is an isotropic fine grained graphite very similar to POCO ZXF-5Q but with a slightly higher density and less uniform porosity [41]. The calculated hardness and modulus of elasticity as a function of depth for all 9 indentations by CSM are shown in Fig. 6. For this set of data the GA fits were done using data from the top 80%–95% of the unloading curve corresponding to the depths at which the CSM data was averaged, although it is important to recognize that the GA uses measurements made during unloading and CSM uses the loading data. Calculated material characteristics were compared to results from fitting the load displacement curve using the Oliver-Pharr method with GA and LSF fitting. The comparison of hardness and elastic modulus values is shown in Fig. 5 and the results from both methods show predominantly the same trends between indentations with somewhat higher values of hardness found using the GA and higher modulus results given by CSM. Material characteristics from LSF are also shown for comparison, the hardness calculated using LSF is extremely similar to the GA values while the elastic modulus results are somewhat lower than the GA fit results. The average hardness computed with each method is 420.00 ± 92.20 MPa for CSM, 499.89 ± 93.95 MPa for the GA, and 504.07 ± 94.58 MPa for LSF. CSM hardness values are just above the expected values for fine grained, isotropic graphite [35–37], while the GA and LSF values are $\approx 20\%$ larger and closer to the range that has been reported for the Vickers hardness of pyrolitic graphites at 400–650 MPa [42]. The average elastic modulus is 12.84 ± 1.41 GPa given by CSM, 10.85 ± 1.19 GPa by the GA, and 10.56 ± 1.17 GPa by LSF. The GA and LSF results are both within 1σ of values found in the literature [35,38–40], but the CSM values are $\approx 20\%$ larger and align more closely with data from indentations on Gilsocarbon and pyrolytic graphites found in the literature at 10.9–14.7 GPa [36,42–45]. Both the hardness and elastic modulus values follow the same trends across all three methods of calculation with GA and LSF values being more closely aligned with each other compared to CSM. In the case of the elastic modulus calculations the GA gives intermediate results between the extremes of the GA and LSF numbers. It is not surprising that the CSM and Oliver-Pharr fitting results are not in perfect agreement. There are known cases where non-ideality has been observed with both techniques [46,47]. The GA methodology utilized here should be used only on samples where the Oliver-Pharr method is indicated.

3.3. LANL HEA mapping

A high entropy alloy (HEA) sample was selected to compare the GA approach to fitting results obtained from the `Hysitron` software. Electron backscatter diffraction was used to obtain an inverse pole figure map Fig. 7(a) and phase map (b). A row of nanoindentations, indicated by a red dashed line, which contained BCC and FCC crystal structures was selected for the comparison. The fit values for hardness and reduced modulus shown in the highlighted portion of the maps in Fig. 7(c) and (d) are plotted along with the values obtained using the GA method in Fig. 8(a) and (b), respectively. The results of the LSF algorithm used to analyze the fused silica and graphite samples is included for comparison to the GA and `Hysitron` software data. Overall the three methods show the same trends between BCC and FCC regions of the sample, and yield similar results for the hardness and modulus when independently averaged over the BCC and FCC results. Indentations fully within the BCC region (#6, 7, 8) have a hardness of 8.4 ± 0.2 GPa as calculated by the GA compared to 8.4 ± 0.2 GPa (`Hysitron`) and 8.5 ± 0.2 GPa (LSF). The elastic modulus calculated for this region is 252 ± 6 GPa, 253 ± 5 GPa, and 253 ± 5 GPa for the GA, `Hysitron`, and LSF respectively. Indentation # 1–4 and # 10–12 are in the region of FCC material and are similarly consistent for the 3 examined algorithms with a hardness value of 2.86 ± 0.04 GPa

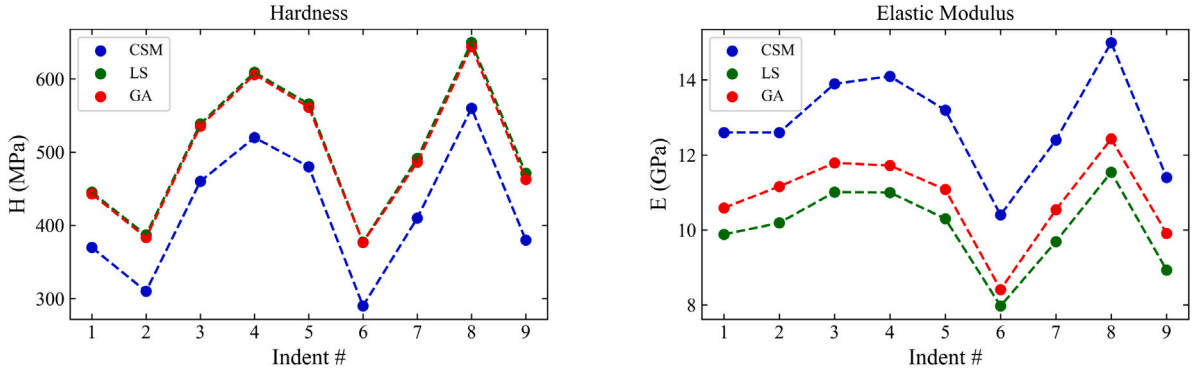

(a) Hardness results (b) Elastic modulus results

Fig. 5. Comparison of hardness and elastic modulus results for IG-430 polycrystalline graphite indentations using CSM. The CSM results (blue) are compared to load displacement analysis using the Oliver-Pharr method fit using the GA (red) and least squares (green) fitting algorithms.

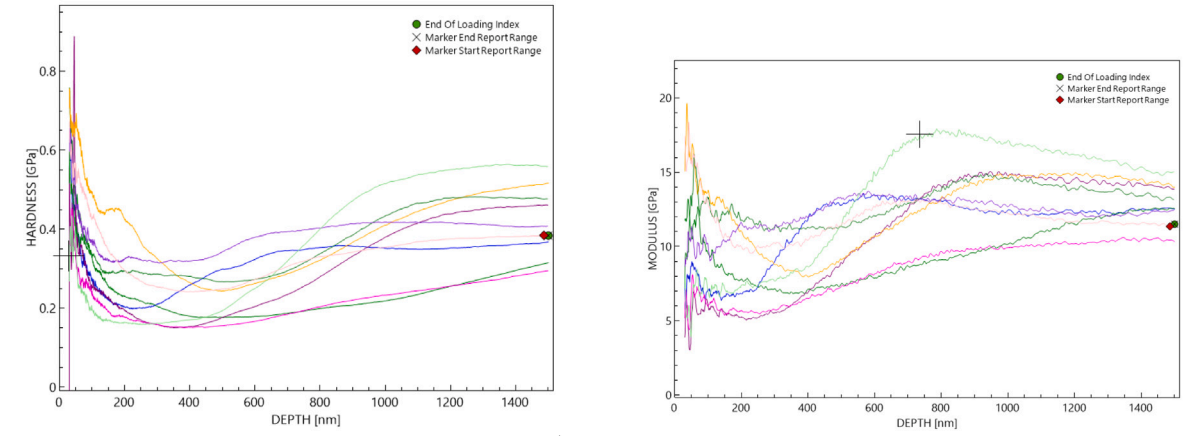

(a) Hardness results for all 9 examined indentations. (b) Elastic modulus results for all 9 examined indentations.

Fig. 6. Nanoindentation CSM results for indentations on pristine IG-430 graphite.

from the GA compared to 2.78 ± 0.05 GPa (Hysitron) and 2.9 ± 0.05 GPa (LSF). The elastic modulus of the FCC region is found to be 184 ± 6 GPa (GA), 183 ± 5 GPa (Hysitron), and 186 ± 3 GPA (LSF). The material characteristics of the 2 different phases of HEA when calculated by 3 different methods all agree within one standard deviation of each other with the exception of the FCC hardness calculated by the Hysitron software which is just below the range of 1σ from the GA and LSF methods. Fig. 7(e) and (f) show the full hardness and reduced modulus maps calculated using our GA software. Comparison to the Hysitron software fit results in Fig. 7(c) and (d) shows good agreement with the GA calculating slightly larger peak hardness and reduced modulus values for the BCC region in the upper right portion of the figure. A typical load/unload curve from indentations in the HEA is shown in Fig. 9. The data from indent # 7 of the highlighted indentations in Fig. 7 is plotted along with the fits produced by our GA (Fig. 9a) and LSF (b). The two fits are extremely similar despite the small differences in the calculated hardness and reduced modulus results as seen in Fig. 8.

3.4. Comparison of genetic algorithm with conventional least squares fitting

The goal of any scientific curve fitting is not to find the best mathematical fit but to find the most physically meaningful fit. By limiting the phase space to be examined to realistic physical parameters, the genetic algorithm can avoid values that are unphysical. As shown in Fig. 4, in the case of graphite, the LSF fit produced an unphysical value for m of approximately 3.02 during the fit at peak load. The GA fit to the same data resulted in a value of approximately 1.91. The ability to limit the fit parameter space to physical values is a big advantage of the genetic algorithm.

Another advantage of the Nanoindentation Neo software is that the fitting process is scriptable so one can readily produce maps of mechanical properties across a material as shown in Fig. 7 without human input. The fitting of all of the points available across the sample can be completely automated.

4. Conclusion

A GA-based Nanoindentation Neo package in our general materials characterization tool Neo framework has been developed for evaluating nanoindentation load displacement data using the Oliver-Pharr method [1]. The Nanoindentation Neo package has been applied to nanoindentation data acquired using Hysitron Triboindenter and KLA iMicro indentation systems for indentations in aluminum and fused silica reference samples, 2 grades of fine grained isotropic graphites, and a high entropy alloy. Results are compared to those computed using a LSF of the unloading curve for the Triboindenter data and CSM for the iMicro data. For the fused silica reference material tests the GA calculates material characteristics that are slightly larger than those found in the literature, but which are consistent with LSF results

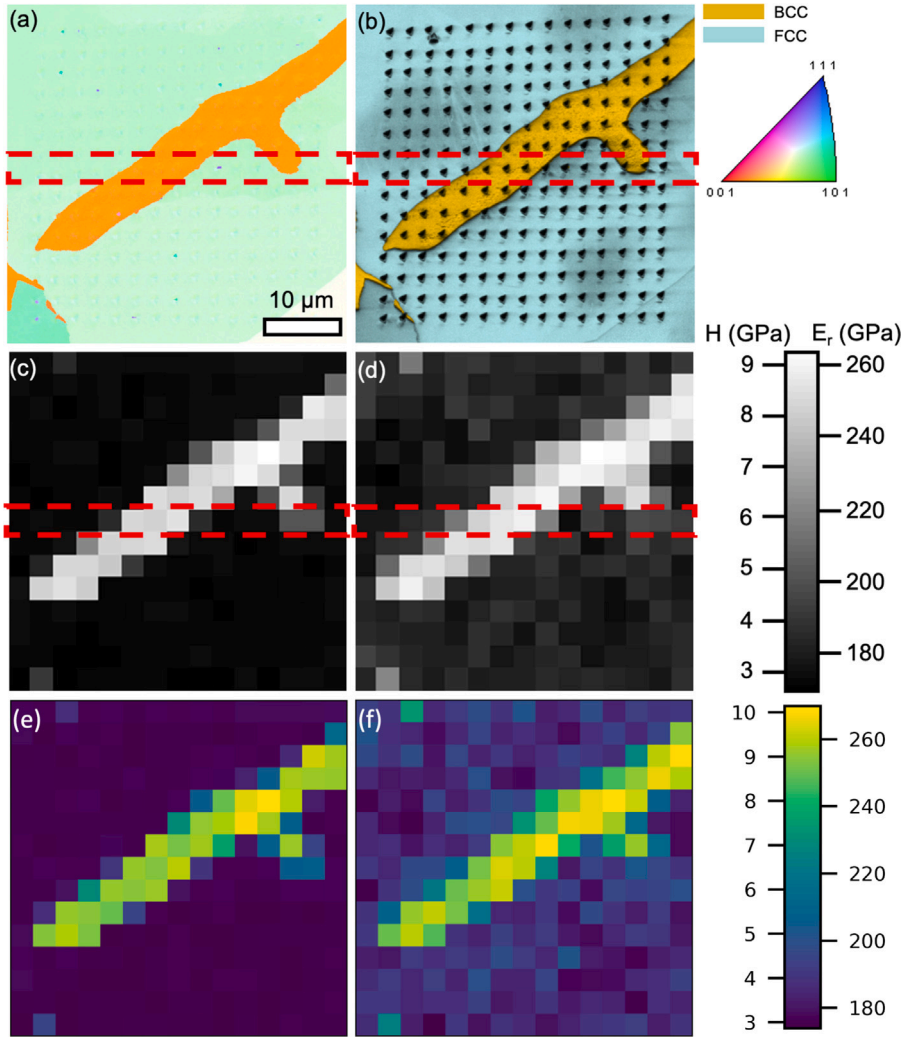

Fig. 7. Maps of HEA sample. Electron backscatter diffraction inverse pole figure (a), and phase map (b) show the higher hardness (c) and reduced modulus (d) values correspond to the BCC structure calculated with the Hysitron software. Mapping of (e) hardness, and (f) reduced modulus using an accelerated GA workflow. A row of nanoindentations, indicated by the red dashed lines are compared in Fig. 8.

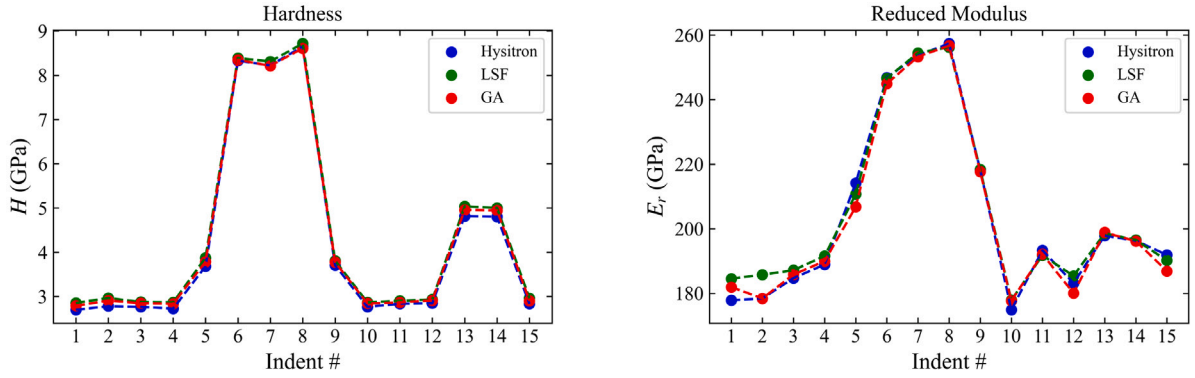

(a) Hardness results (b) Reduced modulus results

Fig. 8. Nanoindentation hardness and elastic modulus result comparison between Hysitron software (blue), GA (red), and LSF (green). The points graphed here correspond to the area indicated by the dashed red line in Fig. 7.

for fits on the same tests. In the case of the aluminum sample the GA results are consistent with those found in the literature, and are 10.5% and 5.7% smaller than the Hysitron software hardness and modulus results respectively. Compared to the LSF, the GA produces fits where the contact geometry parameter m fits well within the range predicted by theory, while the LSF is much above this range for the POCO ZXF-5Q graphite tests. For these tests the elastic modulus computed using the GA is $\approx$ 5% less than those from the LSF, but show the same trends between individual indentations while the hardness results are consistent between the two methods. When comparing GA fitting results to

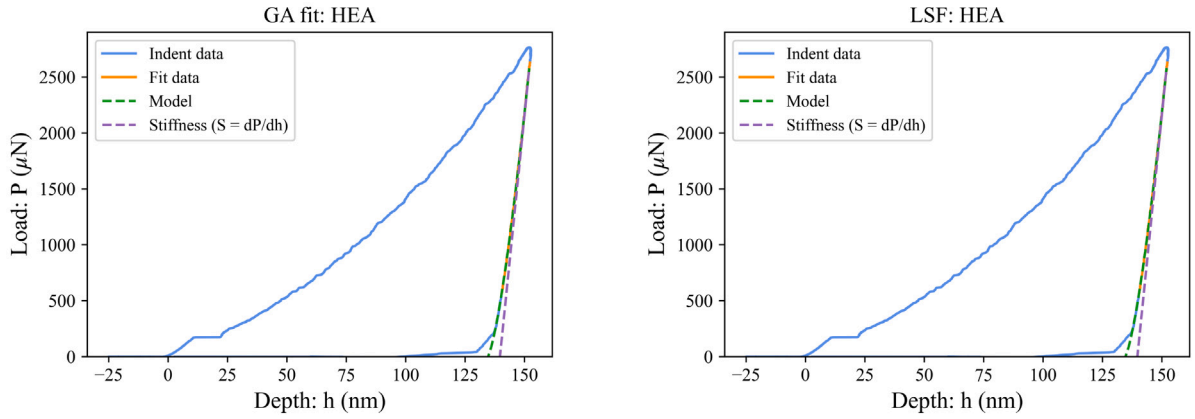

(a) Indentation #7 data with GA fit (b) Indentation #7 data with LSF fit

Fig. 9. Load/unload curve from BCC HEA indentation # 7 of the highlighted row in Fig. 7(a)–(d) with fits calculated using both GA and LSF showing that the two methods produce substantially similar fits.

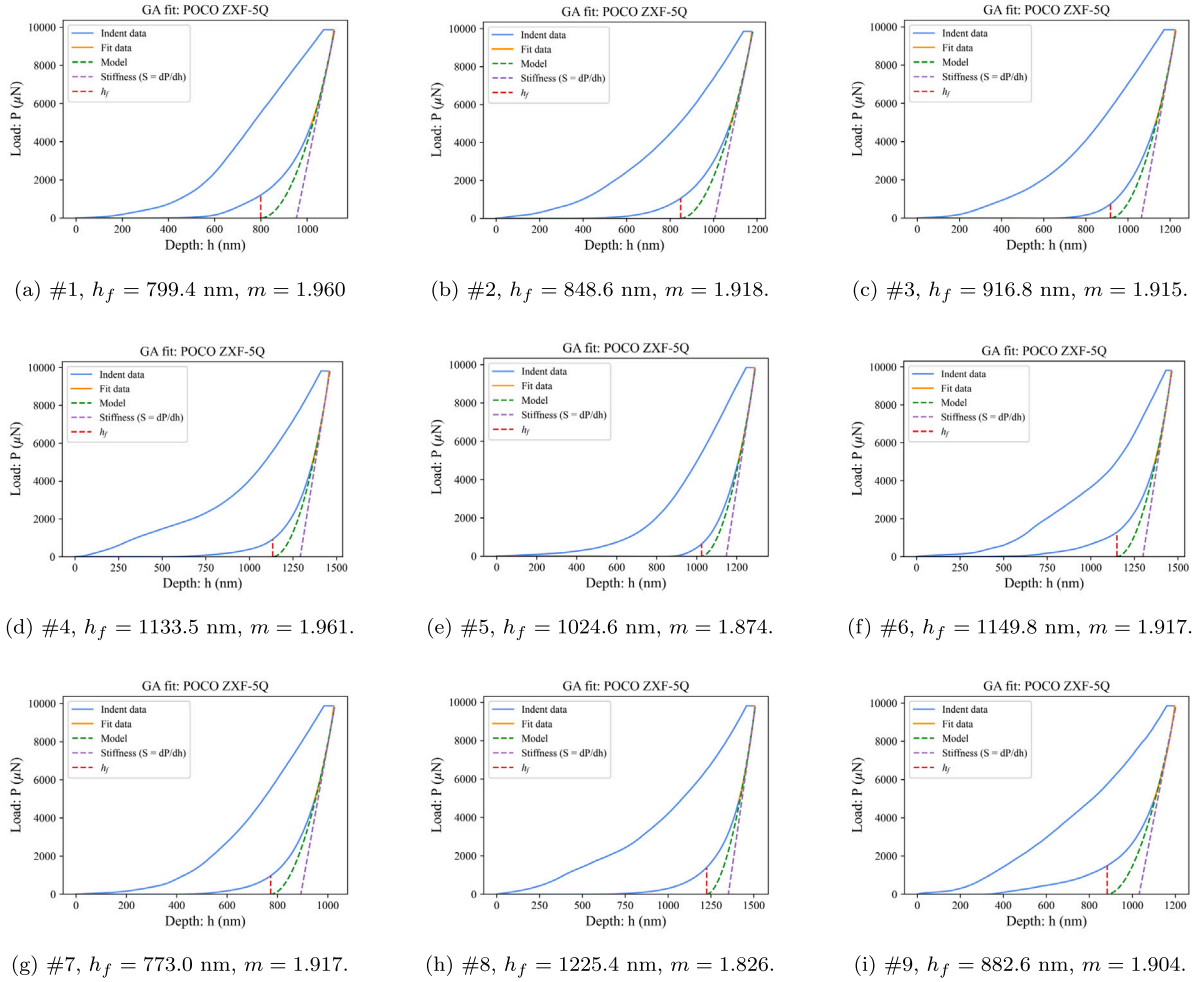

(a) #1, $h_f = 799.4$ nm, $m = 1.960$ (b) #2, $h_f = 848.6$ nm, $m = 1.918$. (c) #3, $h_f = 916.8$ nm, $m = 1.915$.

(d) #4, $h_f = 1133.5$ nm, $m = 1.961$. (e) #5, $h_f = 1024.6$ nm, $m = 1.874$. (f) #6, $h_f = 1149.8$ nm, $m = 1.917$.

(g) #7, $h_f = 773.0$ nm, $m = 1.917$. (h) #8, $h_f = 1225.4$ nm, $m = 1.826$. (i) #9, $h_f = 882.6$ nm, $m = 1.904$.

Fig. 10. Load displacement curves and GA fits for the top half of the unloading curve of all indentations in POCO ZXF-5Q graphite discussed in Section 3.2, the vertical line indicates the corresponding location of h_f on the unloading curve.

CSM measurements the CSM results for elastic modulus are consistently larger for each individual indentation, but the different methods show the same trends across all indentations. The situation is reversed in the case of hardness where the GA values are consistently larger than those from LSF, while the trends between indentations are again consistent. LSF fits of the same data are more aligned with the results of the GA compared to CSM; the LSF and GA hardness plots are overlapping, but the LSF modulus results are somewhat lower than both GA and CSM while again showing the same trends. When applied to indentations in an HEA the GA results were consistent with the `Hysitron` software as well as the LSF algorithm used for analysis of the fused silica and graphite samples. All three fitting algorithms showed the same trends

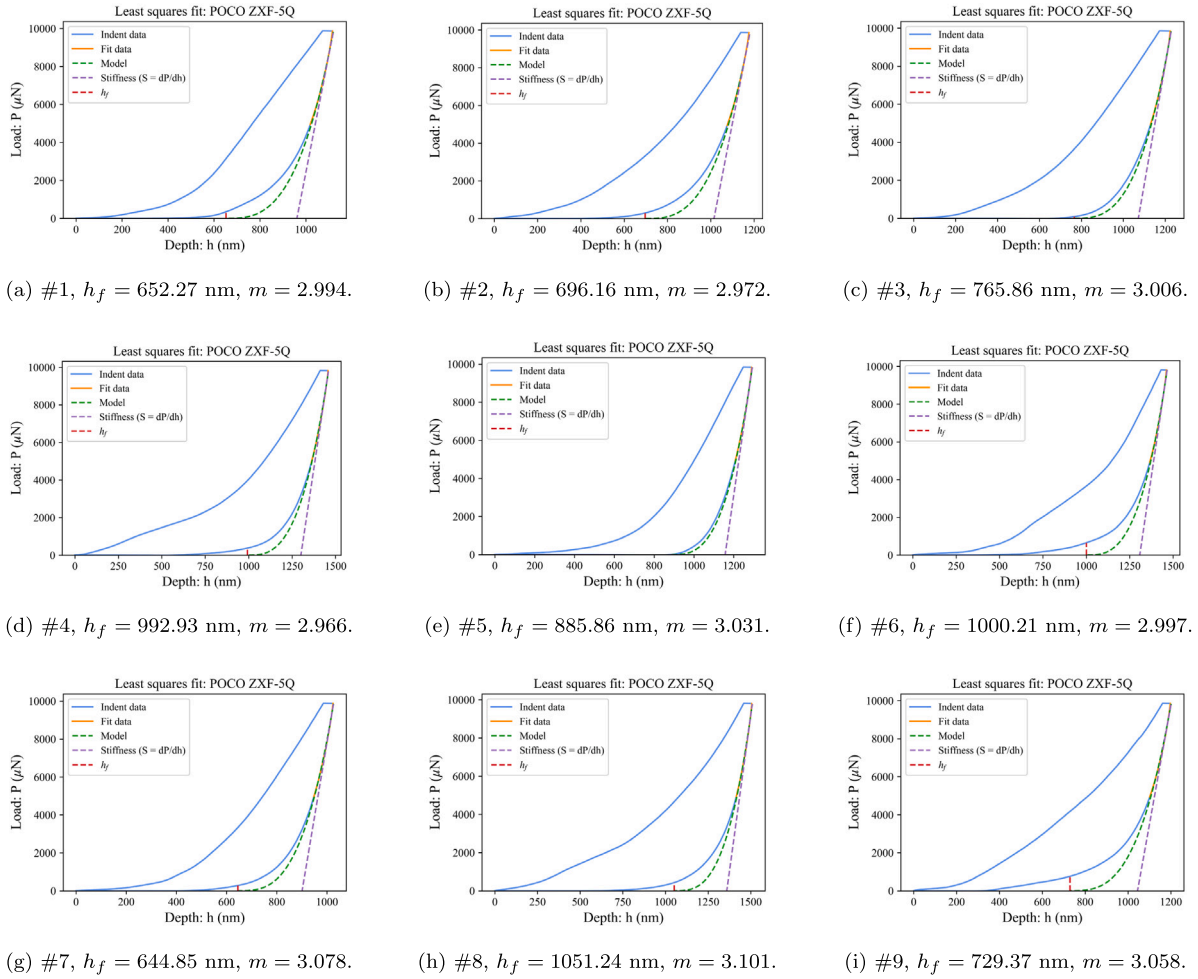

(a) #1, $h_f = 652.27$ nm, $m = 2.994$. (b) #2, $h_f = 696.16$ nm, $m = 2.972$. (c) #3, $h_f = 765.86$ nm, $m = 3.006$.

(d) #4, $h_f = 992.93$ nm, $m = 2.966$. (e) #5, $h_f = 885.86$ nm, $m = 3.031$. (f) #6, $h_f = 1000.21$ nm, $m = 2.997$.

(g) #7, $h_f = 644.85$ nm, $m = 3.078$. (h) #8, $h_f = 1051.24$ nm, $m = 3.101$. (i) #9, $h_f = 729.37$ nm, $m = 3.058$.

Fig. 11. Load displacement curves and Least Squares fits for the top half of the unloading curve of all indentations in POCO ZXF-5Q graphite discussed in Section 3.2, the vertical line indicates the corresponding location of h_f on the unloading curve.

across all tests, and produced consistent estimates for the hardness and modulus of the FCC and BCC phases.

CRediT authorship contribution statement

Abraham Burleigh: Software, Investigation, Formal analysis, Writing – original draft. **Miu Lun Lau:** Software, Investigation, Formal analysis, Writing – original draft. **Megan Burrill:** Software, Investigation, Formal analysis. **Daniel T. Olive:** Conceptualization, Methodology, Validation, Software, Resources, Formal analysis, Project administration, Funding acquisition, Supervision, Writing – review & editing. **Jonathan G. Gigax:** Methodology, Validation, Resources, Formal analysis, Project administration, Funding acquisition, Supervision, Writing – review & editing. **Nan Li:** Methodology, Validation, Resources, Formal analysis, Project administration, Funding acquisition, Supervision, Writing – review & editing. **Tarik A. Saleh:** Methodology, Validation, Resources, Formal analysis, Project administration, Funding acquisition, Supervision, Writing – review & editing. **Frederique Pellemoine:** Methodology, Validation, Resources, Formal analysis, Project administration, Funding acquisition, Supervision, Writing – review & editing. **Sujit Bidhar:** Methodology, Validation, Resources, Formal analysis, Project administration, Funding acquisition, Supervision, Writing – review & editing. **Min Long:** Conceptualization, Methodology, Software, Resources, Project administration, Funding acquisition, Supervision, Writing – review & editing. **Kavin Ammigan:** Conceptualization, Methodology, Software, Resources, Project administration, Funding acquisition, Supervision, Writing – review & editing. **Jeff Terry:** Conceptualization, Methodology, Software, Resources, Project administration, Funding acquisition, Supervision, Writing – review & editing.

Declaration of competing interest

The authors declare that they have no known competing financial interests or personal relationships that could have appeared to influence the work reported in this paper.

Data availability

The code is available under an Open Source license at the repository given in the reference section of the paper.

Acknowledgments

This work was partially supported through Idaho National Laboratory (INL) Laboratory Directed Research and Development (LDRD) Program under U.S. Department of Energy (DOE) Idaho Operations Office Contract DE-AC07-05ID14517. This research made use of the resources of the High Performance Computing Center at Idaho National Laboratory, which is supported by the Office of Nuclear Energy of the U.S. DOE and the Nuclear Science User Facilities under Contract No. DE-AC07-05ID14517. This work was partially supported by the National Science Foundation (Grant No. 2213494). This work was

Table 5
Calibration constants used to determine contact area for the various nanoindentation instruments used in this study.

Sample instrument	Fused silica, POCO NUANCE Hysitron	Aluminum LANL Hysitron	HEA LANL Hysitron	IG-430 KLA iMicro
C_0	24.5	24.5	24.5	19.01889038
C_1	4763.099793	372.37	−17070.94317	8123.641812
C_2	−251703.8989	309350	1667038.537	−1000412.82
C_3	2496563.763	−4269200	−18261922.22	21774959.37
C_4	−6260430.021	12249000	47427195.76	−129554487.7
C_5	4045456.815	−8396900	−31028857.01	253232301.4
C_6	0	0	0	−144510297.2
C_7	0	0	0	0
C_8	0	0	0	0

partially supported by the U.S. DOE through the Los Alamos National Laboratory (LANL). LANL is operated by Triad National Security, LLC, for the National Nuclear Security Administration of U.S. DOE (Contract No. 89233218CNA000001), research presented in this article was supported by the LDRD program of Los Alamos National Laboratory under project number 20210001DR. This work was partially supported by the Center for Integrated Nanotechnologies, an Office of Science User Facility operated for the U.S. DOE Office of Science. The work was partially supported by the Fermi National Accelerator Laboratory, managed and operated by Fermi Research Alliance, LLC under Contract No. DE-AC02-07CH11359 with the U.S. DOE. This material is based upon work supported by the U.S. Department of Energy, Office of Science, Office of High Energy Physics under an Early Career Award to KA. The U.S. Government retains and the publisher, by accepting the article for publication, acknowledges that the U.S. Government retains a non-exclusive, paid-up, irrevocable, world-wide license to publish or reproduce the published form of this manuscript, or allow others to do so, for U.S. Government purposes. This work made use of the SPID facility of Northwestern University's NUANCE Center, which has received support from the SHyNE Resource (NSF ECCS-2025633), the IIN, and Northwestern's MRSEC program (NSF DMR-1720139). This work cleared scientific review at Fermilab as report: FERMILAB-PUB-22-597-AD. The work cleared review at Los Alamos National Laboratory as report: LA-UR-22-28433.

Appendix

The Appendix contains plots of the raw data and fitting results for the indentations discussed in Section 3.2 with graphical representations of the unloading stiffness S and residual indentation depth h_f. Fig. 10 shows the fits found with the GA while Fig. 11 shows those given by Least Squares Fitting. The calibration constants C_0 - C_8 for each instrument used to calculate the contact area using Eq. (4) are listed in Table 5.

References

[1] W.C. Oliver, G.M. Pharr, An improved technique for determining hardness and elastic modulus using load and displacement sensing indentation experiments, J. Mater. Res. 7 (6) (1992) 1564–1583.
[2] J. Back, Physics studies for the LBNF graphite target design, in: Proc. IPAC'21, in: International Particle Accelerator Conference, (12) JACoW Publishing, Geneva, Switzerland, 2021, pp. 3123–3125, http://dx.doi.org/10.18429/JACoW-IPAC2021-WEPAB212.
[3] X. Ding, H. Kirk, K.T. McDonald, Particle production of a graphite target system for the intensity frontier, 2015.
[4] T. Nakadaira, T. Haruyama, K. Kasami, S. Koike, A. Ichikawa, C. Densham, M. Fitton, V. Francis, M. Rooney, T2K target, AIP Conf. Proc. 981 (1) (2008) 290–292.
[5] M. Bonesini, A. Marchionni, F. Pietropaolo, T. Tabarelli de Fatis, On particle production for high energy neutrino beams, Eur. Phys. J. C - Particles Fields 20 (1) (2001) 13–27.
[6] L. Aliaga, M. Kordosky, T. Golan, O. Altinok, L. Bellantoni, A. Bercellie, M. Betancourt, A. Bravar, H. Budd, M. Carneiro, et al., Neutrino flux predictions for the NuMI beam, Phys. Rev. D 94 (9) (2016) 092005.
[7] C. Schubert, H. Bahr, H. Weiss, Crack propagation and thermal shock damage in graphite disks heated by moving electron beam, Carbon 24 (1) (1986) 21–28.
[8] J. Pethica, R. Hutchings, W. Oliver, Philos. mag. a, 1983.
[9] W. Oliver, R. Hutchings, J. Pethica, P. Blau, B. Lawn, ASTM STP 889, American Society of Testing and Materials. Philadelphia, PA (1986) 90–108.
[10] I.N. Sneddon, The relation between load and penetration in the axisymmetric Boussinesq problem for a punch of arbitrary profile, Internat. J. Engrg. Sci. 3 (1) (1965) 47–57.
[11] A. Temovskii, V. Alekhin, M. Kh, Shorshorov, Konshov, MM and Skvortsov, VN, Zavod. Lab 39 (1973) 1242.
[12] S. Bulychev, V. Alekhin, M.K. Shorshorov, A. Ternovskij, G. Shnyrev, Determination of Young modulus by the hardness indentation diagram, Zavod. Lab. 41 (9) (1975) 1137–1140.
[13] S. Bulychev, V. Alekhin, M.K. Shorshorov, et al., Study into the mechanical properties of materials using the kinetic loading–impression depth curve under microindentation, Probl. Prochn (9) (1976) 79–83.
[14] M.K. Shorshorov, S. Bulychev, V. Alekhin, Work of plastic and elastic deformation during indenter indentation, in: Soviet Physics Doklady, Vol. 26, 1981, p. 769.
[15] S. Bulychev, V. Alekhin, Method of kinetic hardness and microhardness in testing impression by an indentor, Ind. Lab. 53 (11) (1988) 1091–1096.
[16] G. Pharr, W.C. Oliver, F. Brotzen, On the generality of the relationship among contact stiffness, contact area, and elastic modulus during indentation, J. Mater. Res. 7 (3) (1992) 613–617.
[17] J. Harding, I. Sneddon, The elastic stresses produced by the indentation of the plane surface of a semi-infinite elastic solid by a rigid punch, in: Mathematical Proceedings of the Cambridge Philosophical Society, Vol. 41, (1) Cambridge University Press, 1945, pp. 16–26.
[18] R. King, Elastic analysis of some punch problems for a layered medium, Int. J. Solids Struct. 23 (12) (1987) 1657–1664.
[19] J. Pethica, W. Oliver, Tip surface interactions in STM and AFM, Phys. Scr. 1987 (T19A) (1987) 61.
[20] W. Oliver, J. Pethica, Method for continuous determination of the elastic stiffness of contact between two bodies, U.S. patent 4 848 141, 1989.
[21] K.-F. Man, K.-S. Tang, S. Kwong, Genetic algorithms: concepts and applications [in engineering design], IEEE Trans. Ind. Electron. 43 (5) (1996) 519–534.
[22] J. Terry, et al., Analysis of extended X-ray absorption fine structure (EXAFS) data using artificial intelligence techniques, Appl. Surf. Sci. 547 (2021) 149059.
[23] M.L. Lau, M. Long, J. Terry, Automated materials spectroscopy analysis using genetic algorithms, in: Springer Nature: Transactions on Computational Science & Computational Intelligence, Springer Nature, 2021.
[24] EXAFS Neo, Open source repository for the EXAFS neo analysis package, 2022, https://github.com/laumiulun/EXAFS-Neo-Public (Retrieved: 02 Nov 2022).
[25] Nanoindentation Neo, Open source repository for the nano neo analysis package, 2021, https://github.com/laumiulun/Nano-Neo-Public (Retrieved: 02 Dec 2022).
[26] D. Thierens, Adaptive mutation rate control schemes in genetic algorithms, in: Proceedings of the 2002 Congress on Evolutionary Computation. CEC'02 (Cat. No. 02TH8600), Vol. 1, IEEE, 2002, pp. 980–985.
[27] Python, About Python, 2020, https://docs.python.org/3/faq/general.html#general-python-faq (Retrieved: 22 Dec 2020).
[28] D.R. Redhouse, Uncertainty Quantification of a Genetic Algorithm for Neutron Energy Spectrum Adjustment, Sandia Report SAND2017-4784C, 2017.
[29] D.R. Redhouse, Uncertainty Quantification of a Genetic Algorithm for Neutron Energy Spectrum Adjustment, Texas A&M University, 2017.
[30] B.D. Beake, J.F. Smith, High-temperature nanoindentation testing of fused silica and other materials, Phil. Mag. A 82 (10) (2002) 2179–2186.
[31] M.D. Michel, F.C. Serbena, C. Lepienski, Effect of temperature on hardness and indentation cracking of fused silica, J. Non-Crystalline Solids 352 (32–35) (2006) 3550–3555.
[32] R.F. Cook, G.M. Pharr, Direct observation and analysis of indentation cracking in glasses and ceramics, J. Am. Ceram. Soc. 73 (4) (1990) 787–817.
[33] P. Filippov, U. Koch, Nanoindentation of aluminum single crystals: Experimental study on influencing factors, Materials 12 (22) (2019) 3688.
[34] G. Simmons, H. Wang, et al., Single crystal elastic constants and calculated aggregate properties, Mass., MIT Press, 1971.

[35] B. Zhang, H. Xia, X. He, Z. He, X. Liu, M. Zhao, X. Zhou, Characterization of the effects of 3-MeV proton irradiation on fine-grained isotropic nuclear graphite, Carbon 77 (2014) 311–318.
[36] D. Liu, K. Mingard, O.T. Lord, P. Flewitt, On the damage and fracture of nuclear graphite at multiple length-scales, J. Nucl. Mater. 493 (2017) 246–254.
[37] W. Qi, Z.-T. He, B.-L. Zhang, X.-J. He, C. Zhang, J.-L. Song, G.-H. Lei, X.-T. Zhou, H.-H. Xia, P. Huai, Behaviors of fine (IG-110) and ultra-fine (HPG-510) grain graphite irradiated by 7 MeV xe^{26+} ions, Nucl. Sci. Tech. 28 (10) (2017) 1–8.
[38] A. Richter, R. Ries, R. Smith, M. Henkel, B. Wolf, Nanoindentation of diamond, graphite and fullerene films, Diam. Relat. Mater. 9 (2) (2000) 170–184.
[39] R. Himawan, M. Haryanto, M.B. Setiawan, Mechanical properties prediction of IG-110 graphite by non-destruction inspection using ultrasonic method, Jurnal Sains Materi Indonesia 20 (3) (2019) 120–125.
[40] J. Gao, W. Yao, Y. Ma, Analytical and numerical study of graphite IG110 parts in advanced reactor under high temperature and irradiation, Nucl. Eng. Des. 305 (2016) 421–432.
[41] M. Jiang, A. El-Turke, G. Lolov, K. Ammigan, P. Hurh, D. Liu, Multiple length-scale microstructural characterisation of four grades of fine-grained graphite, J. Nucl. Mater. 550 (2021) 152876.
[42] A. Kren, T. Protasenya, Determination of the physical and mechanical characteristics of isotropic pyrolitic graphite by dynamic indentation method, Russ. J. Nondest. Test. 50 (7) (2014) 419–425.
[43] D. Liu, B. Gludovatz, H.S. Barnard, M. Kuball, R.O. Ritchie, Damage tolerance of nuclear graphite at elevated temperatures, Nature Commun. 8 (1) (2017) 1–9.
[44] M. Mostafavi, S. McDonald, H. Çetinel, P. Mummery, T. Marrow, Flexural strength and defect behaviour of polygranular graphite under different states of stress, Carbon 59 (2013) 325–336.
[45] B. Marsden, M. Haverty, W. Bodel, G. Hall, A. Jones, P. Mummery, M. Treifi, Dimensional change, irradiation creep and thermal/mechanical property changes in nuclear graphite, Int. Mater. Rev. 61 (3) (2016) 155–182.
[46] X. Li, B. Bhushan, A review of nanoindentation continuous stiffness measurement technique and its applications, Mater. Charact. 48 (1) (2002) 11–36.
[47] G. Pharr, J. Strader, W. Oliver, Critical issues in making small-depth mechanical property measurements by nanoindentation with continuous stiffness measurement, J. Mater. Res. 24 (3) (2009) 653–666.